Journal of ELECTRONIC MATERIALS, Vol. 49, No. 1, 2020
https://doi.org/10.1007/s11664-019-07654-0
© 2019 The Minerals, Metals & Materials Society

TMS2019 MICROELECTRONIC PACKAGING, INTERCONNECT, AND PB-FREE SOLDER

Low-Pressure Silver Sintering of Automobile Power Modules with a Silicon-Carbide Device and an Active-Metal-Brazed Substrate

WON SIK HONG,[1,2] MI SONG KIM,[1] and CHULMIN OH[1]

1.—Electronic Convergence Materials and Device Research Center, Korea Electronics Technology Institute (KETI), #25, Saenari-ro, Bundang-gu, Seongnam-si, Gyeonggi-do 13509, Republic of Korea. 2.—e-mail: wshong@keti.re.kr

To improve the efficiency of power modules in environmentally friendly vehicles, silicon-carbide (SiC) chips and silicon-nitride (Si_3N_4) active metal-brazed (AMB) substrates were bonded by low-pressure silver (Ag) sintering at 220°C and 1 MPa using Ag paste. The initial bond strength of the sintered joint was 35.7 MPa, and the void content and bonding-layer thickness of the sintered joint were 4–7% and 94–99 μm, respectively. To verify the reliability of the silver-sintered joints, we conducted thermal cycling tests (TCTs) and high-temperature storage tests (HTSTs). The bond strength of the SiC chip/ Si_3N_4 AMB substrate after the TCT decreased to 16.9 MPa, but increased to 43.6 MPa after the HTST. Thermomechanical fatigue cracks from the difference in the thermal-expansion coefficient occurred at the sintered joint interface during the TCT, which decreased the sintered joint strength. As the sintering process progressed continuously during the long test time at a high temperature, the densification of the sintered joint increased to 98.4%, which lead to an increase in bonding strength. In this study, a SiC device was sinterbonded to a Si_3N_4 AMB substrate using silver paste at a low pressure, and optimization at a commercialized level was achieved.

Key words: Active-metal-brazed (AMB), automobile, power module, pressure, silicon carbide (SiC), silicon nitride (Si_3N_4), silver sintering

INTRODUCTION

Because of various environmental policies, electric vehicles, hydrogen fuel-cell vehicles and hybrid electric vehicles are developing widely and have been commercialized. Along with this progress, the development of power modules for automobiles is also actively underway.[1,2]

The role of the power module is power conversion (alternating current → direct current, direct current → alternating current), power transformation, power stabilization and power management. Recent power modules use silicon-carbide (SiC) MOS field-effect transistors (MOSFET) or insulated gate bipolar transistor (IBGT) devices for highly efficient power conversion. SiC devices have high band-gap energy, high insulation breakdown voltage and high thermal conductivity, compared with that of silicon (Si) devices. Because of their high switching speed, the power-conversion efficiency, high-temperature operation, high switching frequency and low power loss in wide-band gap (WBG) devices has increased in the automotive industry.[1–3] SiC devices have one disadvantage compared with Si, which is a junction temperature.[4,5] Lead (Pb)-free solder is used to assemble the package module. Because of the high junction temperature of SiC, Pb-free solder alloy cannot be used in the die

(Received June 14, 2019; accepted September 17, 2019; published online September 25, 2019)

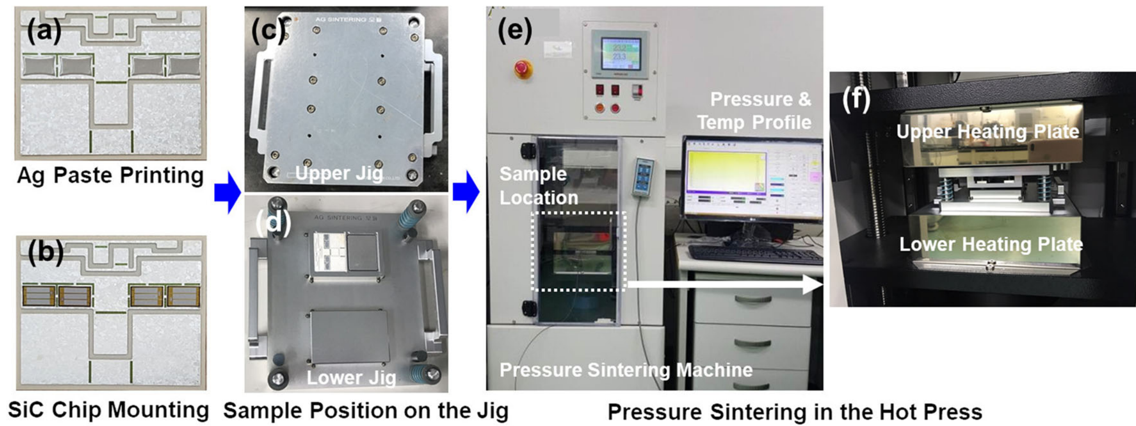

Fig. 1. Photographs of pressurized sintering: (a) Silver-paste printing on a silicon-nitride AMB substrate, (b) SiC chip mounting on a silver-paste printed substrate, (c, d) upper and lower pressure jig, (e) pressure-sintering machine, and (f) magnified view of the sintering jig in between upper and lower heating plate.

attachment materials of SiC device power modules.[4,5] The optimum candidate for new power-module interconnection is silver (Ag)-sintering bonding. A silver-sintering interconnect is the best candidate compared with high-temperature solder alloy bonding (high-temperature soldering) and transient liquid-phase (TLP) bonding because of its high-temperature stability and long-term reliability during operation.[3–9]

Pressure and pressureless methods exist in silver sintering. Pressureless sintering is preferred and it is difficult to maintain the densification and bonding-layer thickness (BLT) of the sintered joint. Pressure sintering applies pressure on the die top area and can achieve a uniform BLT. However, devices can be damaged, such as via cracks because of the direct contact between die tops and pressure tools.

In this study, we optimized the silver sintering of a SiC chip/Si_3N_4 AMB substrate module. Low-pressure silver sintering was performed at a 0.5–1.0 MPa applied pressure with a SiC chip, silicon nitride (Si_3N_4), Ag-plated active metal-brazed (AMB) substrate, and 90 wt% Ag pastes. Low-pressure sintering yielded a maximum 35.7 MPa shear strength and a 7.5% void content of the sintered joint in the as-sintered module. To compare the reliability of the silver-sintered joint, we conducted thermal cycling test (TCT) and high-temperature storage tests (HTST) for 500 cycles and 700 h, respectively. We measured the shear strength and void content of Ag-sintered SiC chip/Si_3N_4 AMB substrate modules using reliability tests, including the TCT and HTST. The microstructure and interface of the SiC/AMB Ag sintered joint were observed using line profiles from scanning electron microscopy (SEM) and energy dispersive x-ray spectroscopy (EDS). Based on these results, we propose a relationship between the shear strength and the void content with the TCT and HTST. We propose a relationship between the BLT and densification in pressurized sintering conditions, and the reliability test methods.

EXPERIMENTAL PROCEDURES

Silicon Carbide Device, Silver Paste and Silicon-Nitride AMB Substrate

Figure 1a and b shows a SiC live device-mounted Si_3N_4 AMB substrate before sintering. SiC devices were used with a 1200 V/200 A, 25-mΩ live MOSFET device (CPM2-1200-0040B, Cree Co., USA) and SiC dummy die. The chip was 180-μm thick, and 4.04 mm wide by 6.44 mm long. The top and back were sputtered with Al (4 μm) and Ni (0.8 μm)/Ag (0.6 μm), respectively.

This study used a commercial silver paste that contained 90 wt% silver powder and 10 wt% binder and activator (CT2700R7S, Kyocera Chemical Co., Japan).

A Si_3N_4 AMB substrate with Ag finish was used. The substrate was 12.0 mm wide, 24.0 mm long and 920-mm thick (0.3 (Cu)/0.32 (ceramic)/0.3 (Cu) mm). The ZTA AMB substrate was composed of Al_2O_3 + ZrO_2 mixed ceramics (Amosense Co., Ltd., Korea), and was 12.0 mm wide, 24.0 m long and 720 mm thick (0.2 (Cu)/0.32 (ceramic)/0.2 (Cu) mm).

The base-plate material was C1220 copper (90.0 mm × 45.0 mm, 3.0 mm thick), which was pre-bent to a 3.20–3.35 mm camber with a 150-μm thickness and a metal mask (stainless steel, SUS304) with a 70% and 80% printing area window.

Low-Pressure Silver-Sintering Condition

Figure 1c and d shows a lower- and upper-pressure jig. The jig was designed to manufacture four samples simultaneously during pressure sintering. Figure 1e shows the pressure-sintering equipment that consisted of a hot press (QM900A-10U, QMESYS Co., Gunpo-si Gyeonggi-do, Korea) and a fixture jig (Fig. 1f). Pressure sintering was performed in air.

Figure 2 shows the temperature and pressure profiles of the pressurized sintering processes. The maximum temperature was held at 220°C for

90 min at 0.5–1.0 MPa in the pre-heating zone. The pressure was released and reapplied from 220°C. At this time, the applied pressure was not continuous, but was released after pressurizing to 0.5 MPa for 10 min in the preheating range. After reaching 220°C, sintering was carried out at 1.0 MPa for 90 min.

Reliability Test Conditions

To compare the reliability of the sintered joints before and after silver sintering, we conducted thermal cycling and high-temperature storage tests.

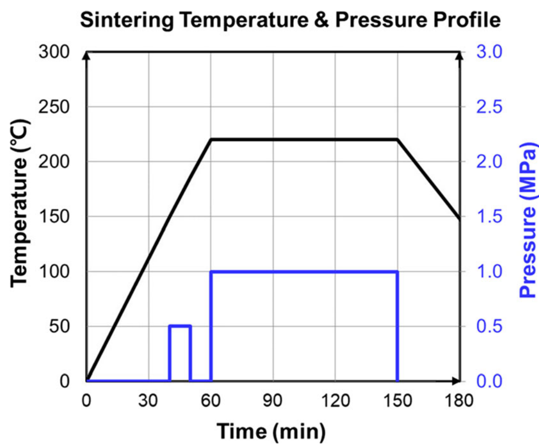

Fig. 2. Temperature and applied pressure profile for silver sintering.

The TCT conditions were − 50°C to 150°C (ΔT = 100°C) with a soak time of 10 min for 500 cycles using a thermal cycling chamber (TSA-11A, ESPEC Co., Japan). HTST was tested at 200 ± 3°C for 700 h using a high-temperature storage oven (OF-22GW, JEIO Tech Co., Japan).

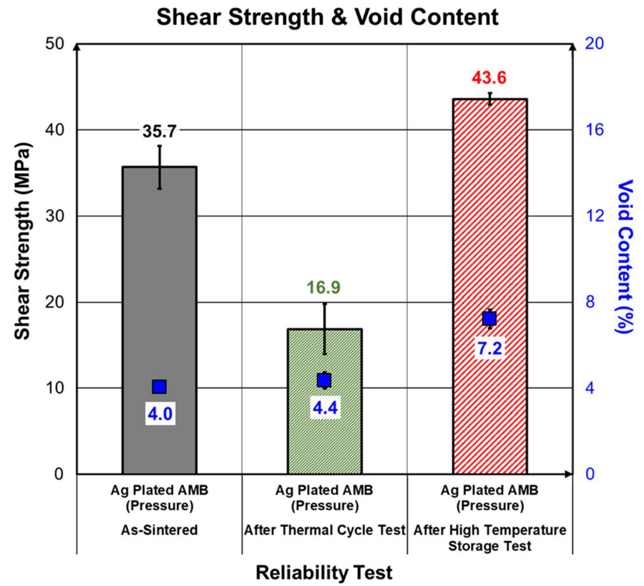

Fig. 4. Shear strength and void content comparison with before/after thermal cycling and high-temperature storage tests.

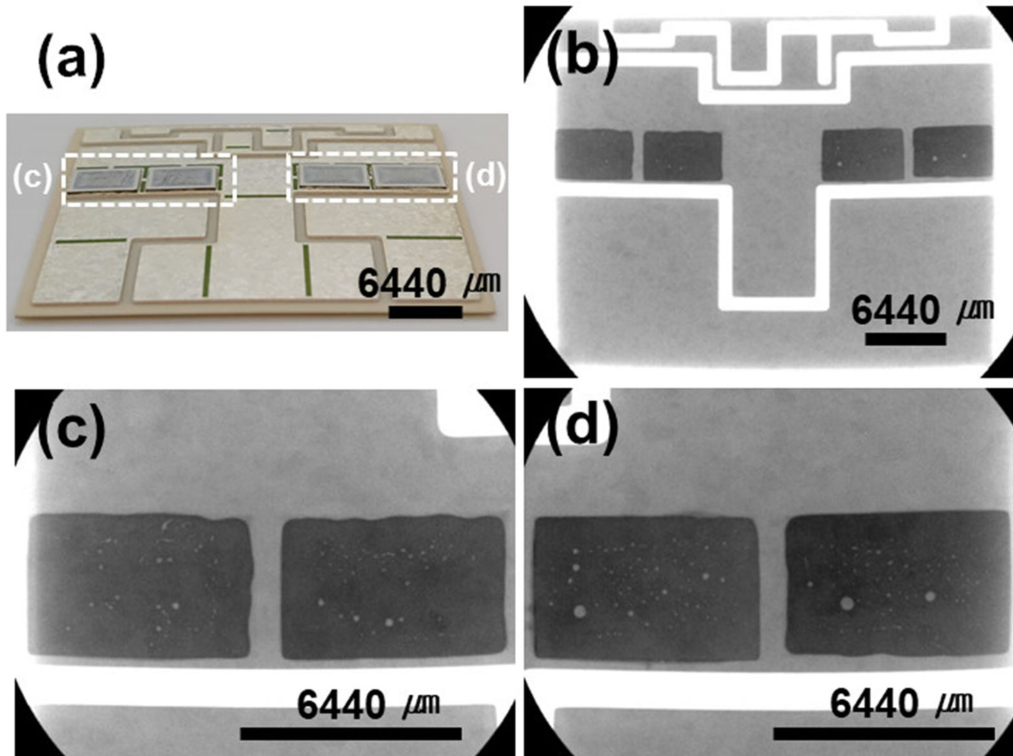

Fig. 3. (a) Photographs and (b–d) x-ray non-destructive analysis images of silver-sintered SiC chip/Si_3N_4 AMB substrate module.

Densification and Shear Strength Measurement of Silver-Sintered Joints

After the pressurized sintering, we examined the cross-sectional area of the silver-sintered joint. We obtained cross-sectional SEM micrographs, and measured the porosity of the silver-sintered joint using *i*-solution software [IMT (Image & Microscope Technology) Inc., USA]. We calculated the densification of the silver-sintered joint as the ratio of porosity and the sintered joint area.

The shear strength was measured by a bonding tester (Dage 4000 model, Nordson DAGE, USA), and was taken as the mean value of the strengths of six sintered samples.

RESULTS AND DISCUSSION

Void Content and Shear Strength of Pressure Silver-Sintered SiC Chip/Si_3N_4 Substrate Joint

Figure 3a shows a photograph of the silver-sintered SiC Chip/Si_3N_4 substrate sample, and Fig. 3b, c, and d are x-ray non-destructive analysis images (Revolution model; X-TEK, UK). In all samples, the void content was 4–8% of the sintered joint layer and a large void was not observed.

Figure 4 compares the shear strength and void content before and after the TCT and HTST. The bond strength of the SiC chip/Si_3N_4 substrate of the as-sintered sample was 35.7 MPa and the void content was 4.0%. The bond strength after the TCT decreased to 16.9 MPa, and that after HTST increased to 43.6 MPa, compared with the initial value. The void contents were 4.4% and 7.2% after the TCT and HTST, respectively. A void content of 10% or less had little influence on the bonding strength. The effect on bond strength was greater for the TCT method compared with the HTST.

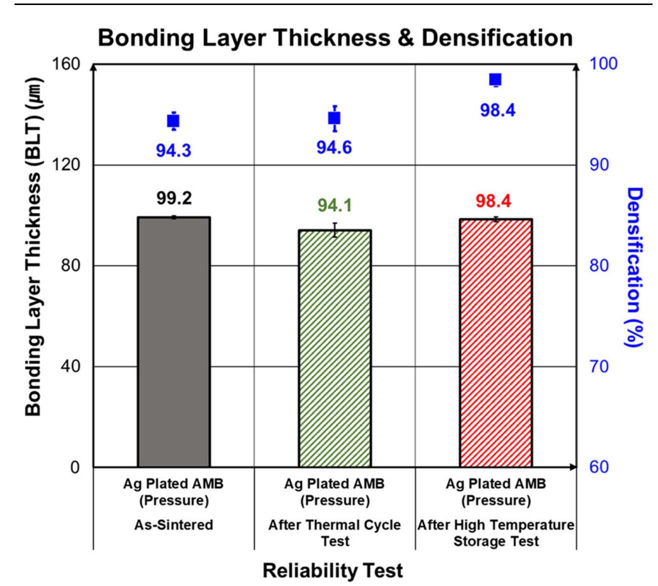

Fig. 6. Bonding layer thickness and densification comparison after the reliability tests.

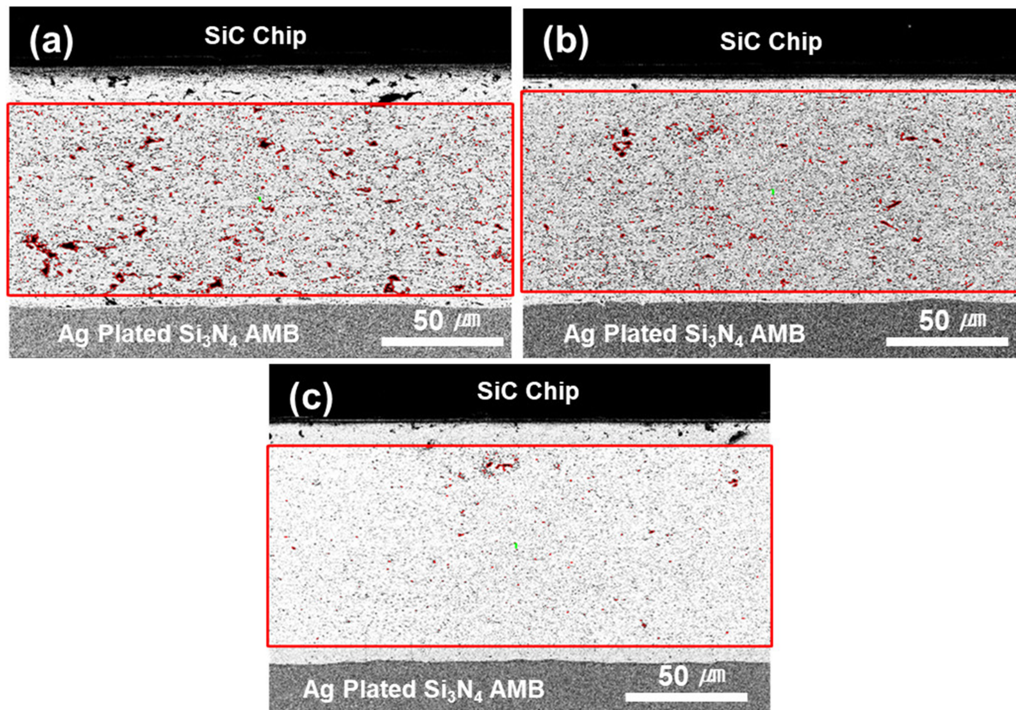

Fig. 5. Cross-sectional SEM micrographs to measure bonding-layer thickness and densification of silver-sintered joints: (a) as-sintered, (b) after 500 thermal cycles and (c) after 700 h high-temperature storage.

Bonding-Layer Thickness, Densification and Microstructure of Low-Pressure Silver-Sintered Joints

Figure 5 shows cross-sectional SEM micrographs that were used to measure the BLT and densification of silver-sintered joints before and after the reliability tests.

As shown in Fig. 6, the initial BLT of the silver-sintered joints was 99.2 μm; after the TCT and HTST, the BLT was 94.2 μm and 98.4 μm, respectively. The BLT appears similar in all samples because those samples were sintered samples under a constant pressure.

The initial densification of the silver-sintered joint from the cross-sectional SEM micrographs in Fig. 5 was 94.3%, and after the TCT and HTST, it was 94.6% and 98.4%, respectively. The densification was similar to that after TCT, whereas the densification after the HTST was increased. Because the TCT can lead to thermomechanical fatigue fracture at the sintered joints due to the difference in thermal-expansion coefficient, the fatigue cracks generate at the joints, and the densification was similar to the as-sintered level. Since the HTST was applied at a high temperature for a long time, densification increased because sintering occurred continuously between the solid-state silver powders during the test. To identify this phenomenon, the microstructure and interfacial analysis of the sintered joints shown in Figs. 7, 8 and 9 were conducted.

Figure 7 shows the SEM images of the as-sintered SiC chip/Si_3N_4 AMB substrate joint and its magnified views. Sintering occurred between the spherical nanopowder and the flake-type micropowder, and a necking structure formed between the silver powders and the interfaces. The general sequence of the solid-state sintering process is the original point contact, neck growth, pore-channel closure, pore rounding, densification and pore shrinkage, and pore coarsening.[10–17] Pores, such as voids, existed between the sintered powders, and pores were observed in the silver-sintered microstructure. As shown in Fig. 7, the densification of the silver-sintered joint was 94.3%, indicating that Ag powder sintering was very well formed.

The SEM images of the Ag sintered joint after HTST are shown in Fig. 8. The densification after the HTST was 98.4%, which was increased to that of the as-sintered joint. The rear of the SiC chip was coated with Ag, and the Ag paste and chip were well sintered with powder as shown in Fig. 8b. Figure 8c shows the magnified image of the silver-sintered joint. Some voids remained unfilled, and micropores were present in the sintered silver powders.

The interface between the silver paste powder and the AMB substrate surface was sintered well (Fig. 8d). The EDS line-profile analysis for the Ag surface finish layer at the AMB substrate interface is shown in Fig. 8e and f. Elemental copper (Cu) was detected in the Ag surface finish layer. The detected Cu is thought to diffuse from the Cu layer of the AMB substrate. Ag was also detected in the Cu

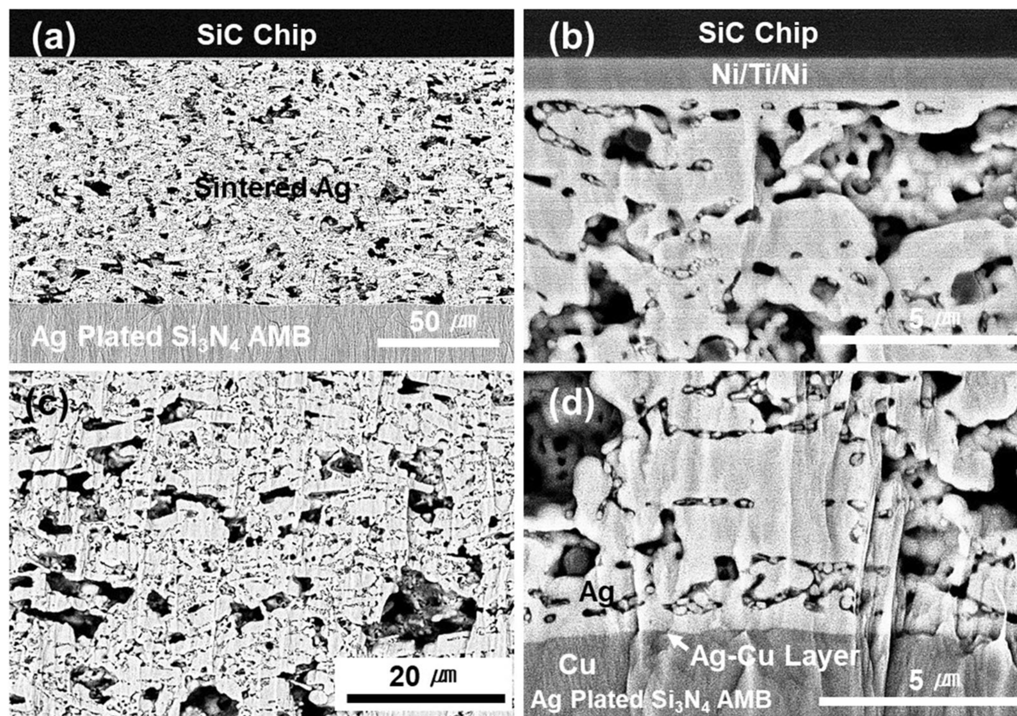

Fig. 7. SEM images of the (a) as-sintered SiC chip/Si_3N_4 AMB substrate joint and a magnified view of the (b) SiC die side, (c) sintered silver joint, and (d) substrate side.

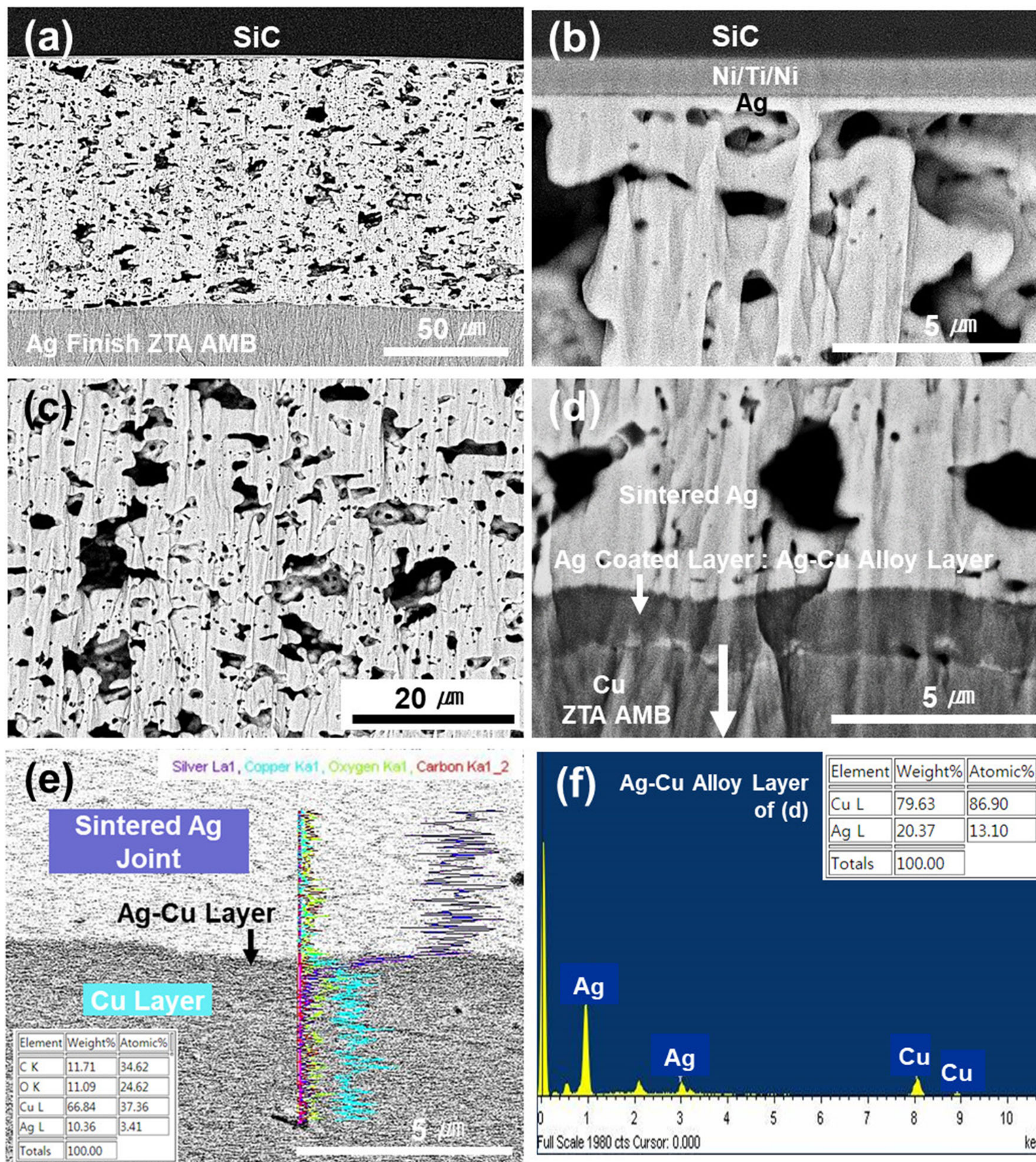

Element	Weight%	Atomic%
C K	11.71	34.62
O K	11.09	24.62
Cu L	66.84	37.36
Ag L	10.36	3.41
Totals	100.00	

Element	Weight%	Atomic%
Cu L	79.63	86.90
Ag L	20.37	13.10
Totals	100.00	

Fig. 8. SEM images of the (a) SiC chip/AMB substrate joint after the high-temperature storage test. (b–d) Magnified view of SiC die, sintered silver joint and substrate side, respectively. (e) Line profile and (f) EDS analysis of Ag-Cu alloy layer of Fig. 6d.

layer that was bound to the Ag surface finish layer. The atomic radii of the Cu and Ag were 0.1278 nm and 0.1444 nm, respectively.[18,19] In the case of Cu-to-Cu and Ag-to-Ag diffusion, grain-boundary diffusivity was higher than that of the lattice diffusion.[18,19] So, Cu and Ag elements have similar diffusion path that is more prevalent than grain-boundary diffusion. Divinski explained that the diffusion rate of Ag through the Cu grain boundaries was higher than that of Cu $\rightarrow$ Ag, and that the Ag $\rightarrow$ Cu alloy layer that formed in the Cu layer was formed more rapidly because the diffusion from Ag $\rightarrow$ Cu was faster under thermal stress.[13] Therefore, as shown in Fig. 8e for the EDS line profile result, it was confirmed that Ag diffused into the Cu layer. The formation of the Ag-Cu alloy layer helped to improve the bonding strength of the silver-sintered joint and contributed to an improvement in the long-term thermal shock reliability of the substrate.

Figure 9 shows a cross-sectional micrograph of the Ag-sintered joint after TCT. Cracks were generated at the edge of the sintered jointed chip, and the cracks propagated along the joint interface. The shape of the crack indicated a traditional fatigue crack mode.[20] Cracks that were generated at the

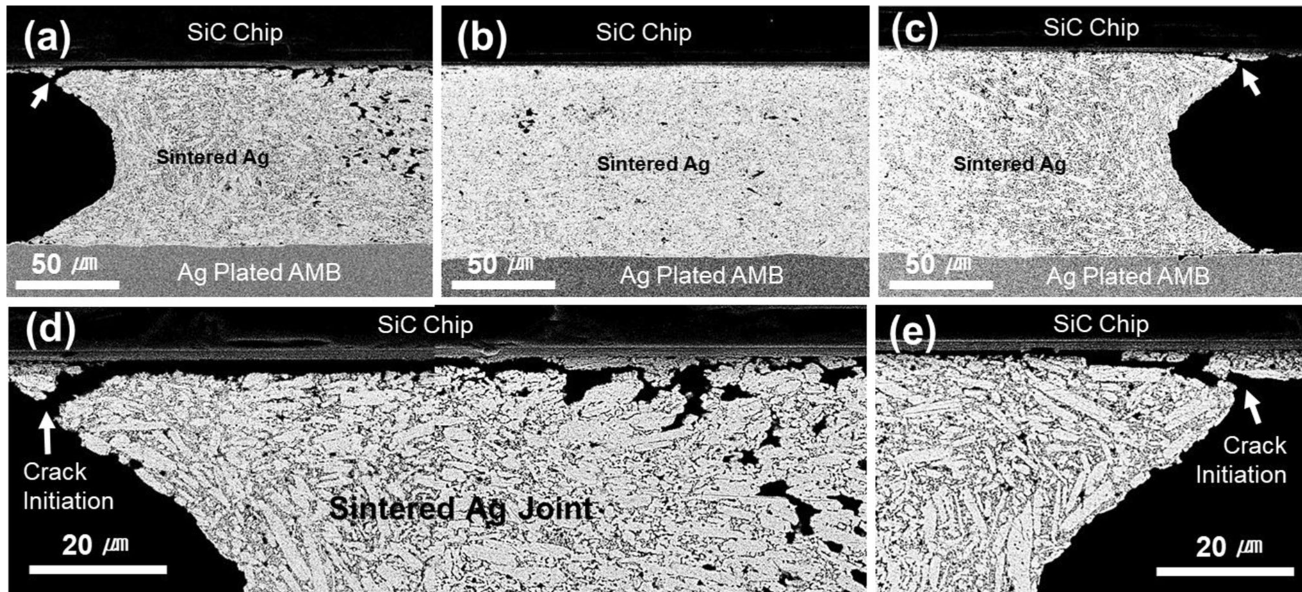

Fig. 9. SEM micrographs of the (a–c) SiC chip/AMB substrate joint after the thermal cycling test. Magnified view of (d) left and (e) right SiC die side, respectively.

sintered joints were observed at the interfaces of the sintered networked powders. During the thermal cycling test, thermomechanical fatigue fracture occurred because of repeated thermal fatigue at high and low temperatures. These joint cracks caused the bond strength after TCT to decrease from the initial 35.7 MPa to 16.9 MPa. During the sintering process, shrinkage of the sintered material may occur due to the particle size (a bigger particle size), shape (smoother surface), densification state, etc. of the powder.[20,21] However, in this study, mixed micro- and nano-powders with irregular and flake shape was used, so the effect of shrinkage seemed small. In addition, during the sintering process, as the binder and the activator evaporated, a very small pressure was additionally applied so that diffusion between the powders occurred quickly, thereby increasing the contact area of the powder. Therefore, to improve the reliability of the silver-sintered joints, it is important to increase the densification rate of the sintered joints and to minimize the unsintered areas.

CONCLUSIONS

Low-pressure silver sintering was optimized using a SiC chip and Si_3N_4 AMB substrate at 220°C, 90 min and a 1-MPa applied pressure in the ambient. The void content and bond strength of the initial SiC chip/Si_3N_4 AMB substrate sintered joints were 4–7% and 35.7 MPa, respectively, and showed an excellent sintered state. The BLT of the pressurized sintered joint was maintained at a constant thickness of 94–99 μm. To verify the reliability of the sintered joints, the shear strength, BLT and densification were measured after the TCT and HTST. The shear strengths were 16.9 MPa and 43.6 MPa after the TCT and HTST, respectively. The shear strength after the HTST was increased compared to the initial strength. Because sintering progresses continuously during the long test time at a high temperature, the densification of the sintered joint increased to 98.4%, which lead to an increase in the bonding strength. Cracks occurred after TCT at the sintered joint interface, and the crack propagated inside along the joint interface between the SiC chip and sintered silver, which caused the joint strength to decrease to 16.9 MPa. Therefore, it is important to increase the densification and increase the bonding strength to improve the reliability of the sintered joint for automobile power modules. In this study, SiC devices were sintered on a Si_3N_4 AMB substrate using silver paste under pressurized conditions, and optimization at a commercialized level was achieved.

ACKNOWLEDGMENTS

This research was supported by the Korea Evaluation Institute of Industrial Technology (KEIT) and the Ministry of Trade, Industry & Energy (MOTIE) of the Republic of Korea (No. 10063263).

REFERENCES

1. S. Ryu, B. Hull, S. Dhar, L. Cheng, Q. Zhang, J. Richmond, M. Das, A. Agarwal, J. Palmour, A. Lelis, B. Geil, and C. Scozzie, *Mater. Sci. Forum* 645, 969 (2010).
2. J. Millan, in *Semiconductor Conference* (*CAS*) (2012), p. 57.
3. W.S. Hong, M.S. Kim, D. Kim, and C. Oh, *J. Electron. Mater.* 48, 122 (2019).
4. H. Zhang, W. Li, Y. Gao, H. Zang, J. Jiu, and K. Suganuma, *J. Electron. Mater.* 46, 5201 (2017).
5. H. Chin, K. Cheong, and A. Ismail, *Metall. Mater. Trans. B* 41, 824 (2010).
6. M. Abtew and G. Selvaduray, *Mater. Sci. Eng. R Rep.* 27, 95 (2000).

7. S.W. Yoon, M.D. Glover, and K. Shiozaki, *IEEE Trans. Power Electron.* 28 (5), 2448 (2013).
8. J.W. Yoon, J.H. Bang, Y.H. Ko, S.H. Yoo, J.K. Kim, and C.W. Lee, *J. Microelectron. Packag. Soc.* 21, 1 (2014).
9. M.S. Kim, C. Oh, and W.S. Hong, *J. Weld. Join.* 37, 15 (2019).
10. J.S. Horschhorn, *Introduction to Powder Metallurgy* (La Vista: The Colonial Press Inc., 1969), pp. 155–273.
11. R.H.R. Castro and K. Benthem, *Sinering* (New York: Springer, 2013), pp. 1–96.
12. S.-K. Lin, S. Nagao, E. Yoko, C. Oh, H. Zhang, Y. Liu, S. Lin, and K. Suganuma, *Sci. Rep.* 6, 34769 (2016).
13. C. Oh, S. Nagao, T. Kunimune, and K. Suganuma, *Appl. Phys. Lett.* 104, 161603 (2014).
14. C. Oh, S. Nagao, and K. Suganuma, *J. Mater. Sci.: Mater. Electron.* 26, 2525 (2015).
15. S. Noh, H. Zhang, and K. Suganuma, *Materials* 11, 2531 (2018).
16. S. Noh, C. Choe, C. Chen, H. Zhang, and K. Suganuma, *J. Mater. Sci.: Mater. Electron.* 29, 15223 (2018).
17. W.S. Hong and S.S. Cha, *J. Microelectron. Packag. Soc.* 19, 67 (2012).
18. S. Divinski, M. Lohmann, and C. Herzig, *Acta Mater.* 49, 249 (2001).
19. R. Shioda, Y. Kariya, N. Mizumura, and K. Sasaki, *J. Electron. Mater.* 46, 1155 (2017).
20. D.R. Gomes, A.A. Turkin, D.I. Vainchtein, and J.M. Hosson, *Scr. Mater.* 164, 17 (2019).
21. C.A. Yang, C.R. Kao, and H. Nishikawa, *2017 IEEE 67th ECTC*, 1974 (2016).

Publisher's Note Springer Nature remains neutral with regard to jurisdictional claims in published maps and institutional affiliations.